Hindawi
Bioinorganic Chemistry and Applications
Volume 2023, Article ID 8892099, 11 pages
https://doi.org/10.1155/2023/8892099

Research Article

Precise Construction of Dual-Promising Anticancer Drugs Associated with Gold Nanomaterials on Glioma Cancer Cells

P. Baby Shakila,[1] Abdurahman Hajinur Hirad,[2] Abdullah A. Alarfaj,[2] Samer Hasan Hussein-Al-Ali,[3] and Beza Mulugeta[4]

[1]*Department of Biochemistry, Vivekananda College of Arts and Sciences for Women, Tiruchengode 637205, Tamil Nadu, India*
[2]*Department of Botany and Microbiology, College of Science, King Saud University, P.O. Box 2455, Riyadh 11451, Saudi Arabia*
[3]*Department of Chemistry, Faculty of Science, Isra University, Amman 11622, Jordan*
[4]*Department of Food Science and Postharvest Technology, Haramaya Institute of Technology, Haramaya University, Dire Dawa, P.O. Box 128, Ethiopia*

Correspondence should be addressed to Beza Mulugeta; beza.mulugeta@haramaya.edu.et

Received 1 June 2023; Revised 5 October 2023; Accepted 10 October 2023; Published 25 October 2023

Academic Editor: Massimiliano F. Peana

Multiple chemodrugs with nanotechnology have proven to be an effective cancer treatment technique. When taken combined, cabazitaxel (CTX) and cisplatin (PT) have more excellent cytotoxic effects than drugs used alone in the chemotherapy of several different cancers. However, several severe side effects are associated with using these chemotherapy drugs in cancer patients. Gold nanomaterials (AuNMs) are promising as drug carriers because of their small diameter, easy surface modifications, good biocompatibility, and strong cell penetration. This work aimed to determine the CTX and PT encapsulated with AuNMs against human glioma U87 cancer cells. The fabrication of the AuNMs achieved a negative surface charge, polydispersity index, and the mean sizes. The combined cytotoxic effect of CTX and PT bound to AuNMs was greater than that of either drug alone when tested on U87 cells. The half inhibitory concentration (IC_{50}) values for free PT were 54.7 μg/mL (at 24 h) and 4.8 g μg/mL (at 72 h). Results acquired from the MTT assay show cell growth decreases time- and concentration-dependent AuNMs, free CTX, free PT, and AuNMs@CTX/PT-induced cytotoxicity and, ultimately, the cell death of U87 cells via apoptosis. The biochemical apoptosis staining techniques investigated the cells' morphological changes of the cells (acridine orange and ethidium bromide (AO-EB) and nuclear staining (DAPI) techniques). The AO-EB and nuclear staining results reveal that the NPs effectively killed cancer cells. Furthermore, the flow cytometry analysis examined the mode of cell death. Therefore, AuNMs@CTX/PT has excellent potential in the cancer therapy of different cancer cells.

1. Introduction

Globally, cancer is a significant public health issue. Every year, more than eleven million people are diagnosed with different cancers [1–5]. With an annual prevalence of 6.6 per 100,000 people worldwide, gliomas are the most widespread primary tumours of the central nervous system (CNS). They arise from glial cells (ependymal, oligodendrocytes, or astrocytes) [6–8]. Gliomas are the most common malignant brain tumour, around 80% in total [9]. WHO categorizes gliomas into four distinct stages. With its high recurrence rate and widespread tumour cell infiltration into the brain parenchyma, glioblastoma multiforme (GBM) is the most common and dangerous form of malignant gliomas [10–12]. There are 3.19 new cases of GBM for every 100,000 people in the United States. Patients treated according to current guidelines had a median survival duration of 14.6 months after diagnosis and a 5-year survival rate of 9.8% [13]. The current treatment protocol includes tumour resection surgery, radiation therapy (RT), and temozolomide chemotherapy as adjuvant therapy [14]. However, the infiltrative high-grade gliomas, which invade vital brain structures, and the lack of clarity in tumour margins pose challenges to the complete resection of gliomas [15]. The invasive glioma cells

frequently form secondary tumours within a few centimetres of the tumour site after surgery. However, most anticancer drugs cannot cross the blood-brain barrier (BBB); hence, chemotherapy only shows limited clinical advantages [16]. Tight connections between endothelial cells, pericytes, and the end foot of astrocytes make up the BBB and control the flow of chemicals into the brain from the circulatory system [17]. So, most therapeutic and diagnostic agents do not get too high enough concentrations in the tumour microenvironment. Two examples of intervention tactics are temporary rupture of the direct drug delivery and BBB by intracerebral injection [18]. However, they are both extraordinarily invasive and unsuitable for long-term treatment. Furthermore, reducing chemotherapy's effectiveness are the drugs' short half-lives and poor solubility in blood circulation [19]. However, the cumulative dosage of radiation that may be securely delivered to keep the accompanying toxicities in the normal tissues acceptable limits the extent to which RT can be applied [20].

Considering the limitations of current glioma diagnosis and treatment methods, nanomedicine has emerged as a potentially effective replacement [21–23]. Gold nanomaterials (AuNMs) have garnered considerable interest among the numerous systems utilized due to their tunable surface functions, unique optical properties, synthetic adaptability, and biocompatibility [23]. The high surface-to-volume ratio of nanomaterials allows for their rapid uptake of imaging contrast agents, drugs, and biomolecules. Therefore, AuNMs have been used for many theranostics applications, such as imaging (e.g., surface-enhanced Raman scattering, magnetic resonance, photoacoustic, and computed tomography), drug administration (e.g., siRNAs and proteins), and drug therapy (e.g. RT, and photothermal therapy) [24–26]. Generally, theranostics is a bridge between diagnostic and therapeutic approaches. In imaging-guided therapy, AuNMs enable microsurgical excision of tumours at a submillimeter spatial resolution, monitor drug administration, and delineate glioma margins with great sensitivity [27–29]. Several research groups reported drug-loaded gold nanomaterials for treating different cancer cells, which shows severe adverse effects [23–25]. Recently, Wan et al. have described the anticancer effects of docetaxel conjugated AuNMs, where the samples show greater cytotoxicity against the HepG2 liver cancer cell line and exposed to have enhanced bioavailability at the tumor site [30].

Castration-resistant prostate cancer can be treated with cabazitaxel (CTX), a second-generation semisynthetic taxanelicensed by the FDA and the European Drugs Agency [31]. The first-generation taxane treatments (such as paclitaxel and docetaxel) have limited utility [32]. Docetaxel and paclitaxel are high-affinity substrates for ATP-dependent multidrug-resistant pumps. Because of difficulties with endothelial influx/efflux ratios, tumour-induced activation of multidrug-resistant pumps decreases effective concentrations of therapeutic and drug penetrations around the BBB [33]. The reduced attraction of multidrug-resistant pumps for cabazitaxel compared to paclitaxel and docetaxel suggests that it will be more effective against brain malignancies [34]. Recent studies have also demonstrated in vivo that cabazitaxel is widely distributed throughout the brain and may be taken up by BBB endothelial cells [35, 36].

Glioma is treated with cisplatin, also known as *cis*-diamminedichloroplatinum (II), one of the most effective chemotherapeutics for the treatment of testicular, ovarian, neck, and head tumours and in neoadjuvant or adjuvant therapy of other tumours [37]. Cisplatin primarily interacts with DNA purine bases to inhibit tumour cell growth and induce death, producing DNA-protein and DNA-DNA interstream and intrastrain crosslinks [38–40]. Combining cisplatin with other chemotherapeutics, such as Gleevec, Paclitaxel, or Gemcitabine, has been shown to sensitize many tumour cell types to cisplatin, hence overcoming cisplatin resistance and toxicity [41]. Metformin has been shown to enhance the response to cisplatin-free treatment and potentate cisplatin-mediated killing of epithelial cancer cells in vitro, making it promising for combining cisplatin-based therapy [42]. However, research into the cytotoxic efficacy of the metformin/cisplatincombination in treating various cancer cell lines is still in its infancy [43].

Researchers are currently focusing on bettering glioma cancer treatments by exploring a variety of therapy methods, with an emphasis on nanotechnology. Gold nanomaterials (AuNMs) have many applications in material science and catalysis [44–46]. They also have significant benefits, such as the ability to be easily scaled down to sizes similar to biomolecules, making them more accessible to biological systems [47]. The anti-inflammatory and antitumour properties of AuNMs have piqued scientific interest in their potential as drug carrier systems [48]. In addition, AuNMs can transport chemotherapeutic drugs to their intended sites of action, maximizing therapy efficacy while minimizing side effects. It is worth noting that studies combining CTX and PT were not discovered, although several studies were reported of using either drug alone in conjunction with gold nanomaterials (Figure 1). This work examined the cytotoxicity of AuNMs coupled with CTX and PT on glioma cells by synthesis, characterization, and in vitro cytotoxicity assessment. In addition, the biochemical apoptosis staining techniques investigated the cells' morphological changes of the cells (AO-EB and DAPI techniques). Furthermore, the flow cytometry analysis examined the mode of cell death. Therefore, AuNMs@CTX/PT has excellent potential in the cancer therapy of different cancer cells.

2. Experimental Section

2.1. Methods and Materials. Cisplatin (PT), cabazitaxel (CTX), chloroauric acid ($HAuCl_4$), and sodium citrate ($Na_3C_6H_5O_7$) were bought from Aladdin Co., Ltd. 3-(4,5-dimethylthiazol-2-yl)-2,5-diphenyltetrazolium bromide (MTT), dimethyl sulfoxide (DMSO), and phosphate-buffered saline (PBS) were obtained from Sigma-Aldrich (USA). Acridine orange/ethidium bromide (AO/EB) and 4′,6-diamidino-2-phenylindole (DAPI) were ordered from Thermo Fisher Scientific, Inc. (USA). All the chemicals and reagents were used without further purification.

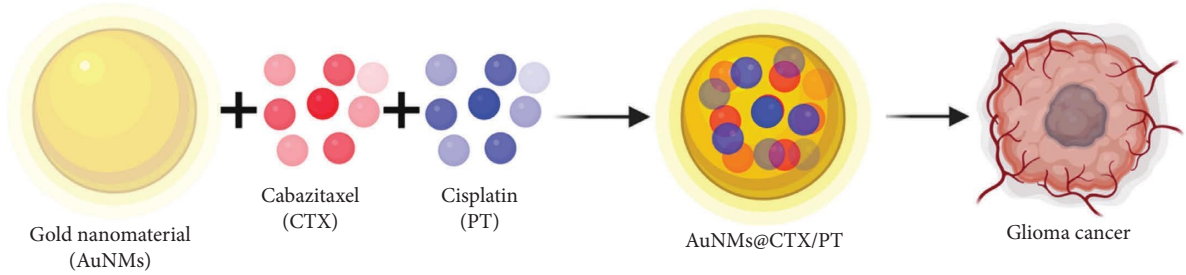

Figure 1: Graphical representation of cabazitaxel (CTX) and cisplatin (PT) associated with gold nanomaterials (AuNMs) fared against human glioma U87 cancer cells.

2.2. Fabrication of AuNMs. The previously reported procedure was successfully used to construct AuNMs [49]. $Na_3C_6H_5O_7$ was used as a reductant and a stabilizer in the chemical reduction of the metal precursor $HAuCl_4$. Under constant stirring, a 1 mM $HAuCl_4$ solution was heated to 95°C. By gradually adding 38 mM $Na_3C_6H_5O_7$ solution (at 50°C), 5 mL of $HAuCl_4$ was converted into AuNMs. Once a solution of the desired purple colour was formed, the reaction was allowed to cool to ambient temperature.

2.3. Construction of AuNMs Containing Drugs. With constant mixing, drug association was carried out with a fixed concentration of CTX or PT in AuNMs solution. A DMSO solution containing 10 μg/mL of CTX and 100 μg/mL of PT was prepared. To facilitate better drug-AuNMs interaction, the solution was agitated at 100 rpm for 24 h (at room temperature). The free drug was extracted from the AuNMs by centrifuging them at 10,000 rpm for 30 minutes.

2.4. Characterization of the Nanomaterials. Samples were prepared by depositing dilute nanoparticle solutions onto carbon film-coated copper grids. TEM images were acquired with an FEI Tecnai F20 TEM (Hillsboro, OR) operating at 200 kV. Nanomaterials were synthesized and then lyophilized to obtain dry samples. The samples were mixed into a KBr pellet at 0.2 wt%. The FTIR spectra of the various nanoparticle samples were obtained using Nicolet 6700 FTIR Spectrometer (Thermofisher, Waltham, MA). The nanomaterial's hydrodynamic size and zeta potential were measured through dynamic light scattering (DLS) via Zetasizer Nano ZS90 (Malvern Instruments, UK). The absorbance was measured at 570 and 630 nm using a microplate reader (Thermo Fisher Scientific, Waltham, MA). UV-vis absorption spectra were recorded using a UV-visible spectrophotometer (Evolution 220, Thermo Fisher Scientific). Cell images were taken using a fluorescence microscope (Olympus CKX53, Japan).

2.5. Quantification of CTX and PT on the AuNMs. UV-vis spectroscopy was used to identify the CTX and PT concentration range in DMSO standard solutions from 0.1 to 5 μg/mL and 10 to 100 μg/mL for the drug quantification tests on the AuNMs. Absorbance was checked at 213 nm (Brix) and 229 nm (CTX) (PT). A calibration curve was obtained for all drugs with an R2 greater than 0.98. The amount of AuNMs precipitated after being centrifuged at 13,000 rpm for 30 minutes was measured. Previous approaches were used to quantify drugs by percentage.

2.6. Anticancer Activity (MTT Assay). The human U87 glioma cancer cells were acquired from the Cell Bank of the Chinese Academy of Sciences (Shanghai, China). U87 cells were cultured in the RPMI 1640 medium supplemented with 10% fetal bovine serum, 100 U of penicillin, and 100 μg/mL streptomycin in a hypoxic chamber (5% CO_2) at 37°C.

The MTT assay assessed the anticancer efficacy of AuNMs, free CTX, free PT, AuNMs@CTX/PT, and in U87 glioma cancer cell lines. After 24 and 72 h of incubation in a 96-well, the cells (2×10^3/each well) were treated with varying doses of the samples. After 24 and 72 h, MTT solution (5 mg/mL) was poured into each well at 10 μL. An additional 4 hours were spent incubating the cells. The formazan crystals were dissolved by removing the excess medium from each well and replacing it with 100 μL of acidified isopropanol. Microplate spectrophotometer (Bio-Tek, USA) readings at 570 nm were used to compile optical density values. Inhibitory concentration (IC_{50}) values were determined using GraphPad Prism 8.0 [50–52].

2.7. Apoptosis Staining. U87 cells were planted at a density of 5×10^3 cells/well in 24-well plates and cultured overnight. AuNMs, free CTX, free PT, and AuNMs@CTX/PT to induce apoptosis in U87 cells were evaluated by the AO/EB double staining method. U87 cells were cultured with AuNMs, free CTX, free PT, and AuNMs@CTX/PT at IC_{50} concentrations. The plates were incubated for 24 and 72 h at 37°C. After 24 h of incubation with an AO/EB staining solution for 5 min, the apoptosis of the U87 cells was analyzed using a fluorescence microscope [53].

Nuclear morphological changes, such as condensation or fragmentation, associated with apoptosis can be assessed by DAPI labelling. U87 cells were seeded at a density of 5×10^3 cells/each well in 24-well plates and incubated overnight. In this assay, U87 cells were incubated of AuNMs, free CTX, free PT, and AuNMs@CTX/PT and incubated for 24 and 72 h at 37°C. Following incubation, the cells were washed twice with PBS, fixed with 4% paraformaldehyde, and rehydrated in 70% ethanol. After incubation with DAPI staining solution and after incubation for 5 min, the

apoptosis of the U87 cells was analyzed using a fluorescence microscope [54–56].

U87 cells were planted at a density of 5×10^3 cells/well in 96-well plates and cultured overnight. After that, the medium was changed with a fresh medium (pH 7.2) including AuNMs, free CTX, free PT, and AuNMs@CTX/PT for 24 and 72 h at IC_{50} concentration. After further incubation for 24 and 72 h, the cells were rinsed thrice with PBS, collected, and dyed with the Annexin V-FITC/PI assay kit. The quantitative apoptosis assay was investigated by flow cytometric investigation [57].

2.8. Statistical Analysis. The data shown here were presented as the mean ± standard deviation (SD). The significance of the deviation was verified by one-way ANOVA, which was significant when $P < 0.05$ and very substantial when $P < 0.01$.

3. Results and Discussion

3.1. Physicochemical Characterization. UV-vis analysis assessed the AuNMs' optical characteristics by monitoring for wavelength shifts caused by drug association. The maximum absorbance wavelength of free AuNMs, which is 526 nm for AuNMs of size 20 nm, was not changed by CTX, as shown in Figure 2(b). Slight wavelength shifts were shown when AuNMs were mixed with PT, indicating a more vital chemical interaction between the carboxylic acid on the AuNMs' surface and the PT. This finding is consistent with drug quantification results reported by UV-vis spectroscopy, which also showed a high level of interaction between AuNMs and PT (88% ± 5%). A combined percentage calculation of AuNMs and CTX yielded 48 ± 5%.

The free AuNMs employed in this work had an average diameter of 20 nm, confirmed by transmission electron microscopy (TEM) (Figure 2(a)). This confirms the accuracy of the UV-vis analysis. As anticipated, the average diameter of AuNMs showed a considerable increase after association with various drugs, indicating that the drugs formed a layer on the surface of the AuNMs. While the polydispersity index for PT-related AuNMs was >0.2, it was narrower for free AuNMs and AuNMs linked with CTX. In addition, drug-AuNMs' interactions changed the charged surface. High zeta potential was observed in the AuNMs, correlated with enhanced colloidal stability. As a result, we can infer that the AuNMs have a stable drug coating and perform well in stability tests. Transmission electron microscopy (TEM) and ultraviolet-visible spectroscopy all corroborated the findings that the drugs had a connection to AuNMs. The mica surface, which the nanomaterials were easily spread throughout, was hydrophilic.

We used Fourier transform infrared spectroscopy (FTIR) to analyze the drug's chemical structure and investigate its potential interactions with AuNMs. Figure 2(c) displays the peak properties of AuNMs, which coincide with the COO's symmetric and asymmetric stretching.

The FTIR spectra of free PT, AuNMs@PT, free CTX, AuNMs@CTX, and AuNMs were noted in the spectral regions at 4000–400 cm^{-1} as demonstrated in Figure 2(c). The FTIR spectra of AuNMs demonstrated the -OH symmetric stretching vibration at 3459.14 $cm^{-1}$and 3268.54 cm^{-1}, representing the presence of the alcoholic group. The presence of the C-H bond was noted at 2845.96 cm^{-1}, and the presence of the C=O bond was recorded at 1610.19 cm^{-1}, 1593.41 cm^{-1}. The bands at 1427.45 cm^{-1} and 1374.57 cm^{-1} fitted to C-C-C stretching, while the wave number 1267.42 cm^{-1} to 1072.47 cm^{-1} indicated the carboxylic C-O groups. The combination of AuNMs and PT showed the signature peaks of AuNMs and the stretching bands at about 3300 and 1297 cm^{-1}. However, no additional peaks were observed. Furthermore, no new peaks were observed in the AuNMs@CTX combination, indicating no chemical interaction between the drugs and the AuNMs.

3.2. In Vitro Cytotoxicity Investigation. As shown in Figure 3, we tested the cytotoxicity of AuNMs, free CTX, free PT, and AuNMs@CTX/PT in U87 cells at varying doses and incubation durations (24 and 72 h). After 24 h (Figure 3) and 72 h (Figure 3) of exposure, U87 cells treated with 0.01, 0.02, 0.03, and 0.04 μg/mL of free CTX and AuNMs@CTX revealed a substantial decrease in U87 cell viability (Figure 3). Both free CTX and AuNMs@CTX reduced cell viability in a concentration-dependent way after 72 h of exposure. Still, there was no other significant difference between the groups. It was shown that although free CTX caused a 27% reduction in cells at a dose of 0.03 μg/mL, AuNMs@CTX caused a 32% reduction. Cell viability decreased by 47% when exposed to free CTX and 50% when exposed to AuNMs@CTX at a dose of 0.04 μg/mL. Despite not having a more potent cytotoxic impact, AuNMs@CTX in the 24 h exposure period demonstrated significant effects compared to free CTX at both the evaluated 0.01 and 0.02 μg/mL dosages. At a 0.01 μg/mL concentration, free CTX reduced cell viability by 18%, whereas AuNMs@CTX reduced viability by 20%. Free CTX decreased cell viability by 29% and AuNMs@CTX by 32% at a 0.02 μg/mL concentration. IC_{50} values for the suppression of U87 cell viability by free CTX and its combination with AuNMs were similar across the tested groups. At the concentration employed in all the studies (10 μg/mL), free AuNMs exhibited no appreciable cytotoxic effect on the U87 cells. U87 cells exposed to AuNMs@PT for 24 h demonstrated a more potent cytotoxic effect than those exposed to free PT, resulting in a concentration-dependent decrease in cell viability (Figure 4). In comparison to the concentrations of 0.3, 0.5, 1.0, and 2.0 μg/mL, the reduction in cell viability for free PT was 9, 5, 8, and 15%, while the reduction in cell viability for AuNMs@PT was 27, 34, 37, and 44%. The half inhibitory concentration (IC_{50}) values for free PT were 54.7 μg/mL (at 24 h) and 4.8 g μg/mL (at 72 h). The IC_{50} value for PT in combination with AuNMs after 24 h of incubation was substantially lower than that of free PT. The MTT assay results suggested that CTX and PT treatment combined with AuNMs had a more significant cytotoxic effect.

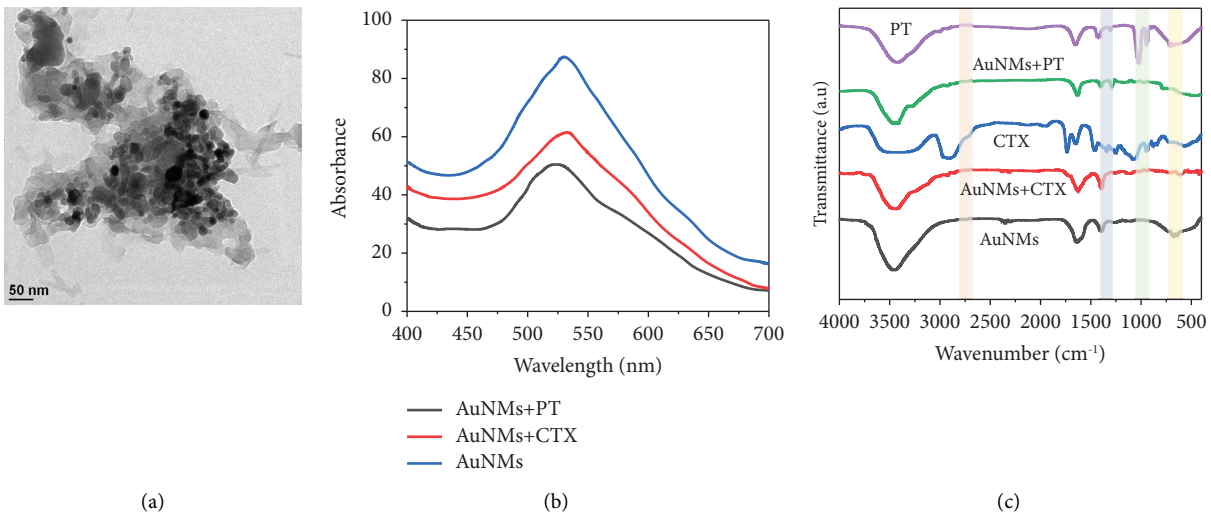

Figure 2: Morphological characterisation of cabazitaxel (CTX) and cisplatin (PT) associated with gold nanomaterials (AuNMs). (a) TEM image of AuNMs@CTX/PT. (b) UV-vis analysis of free AuNMs and AuNMs associated with CTX and PT. (c) FTIR analysis of free AuNMs, PT, CTX, and AuNMs associated with CTX and PT.

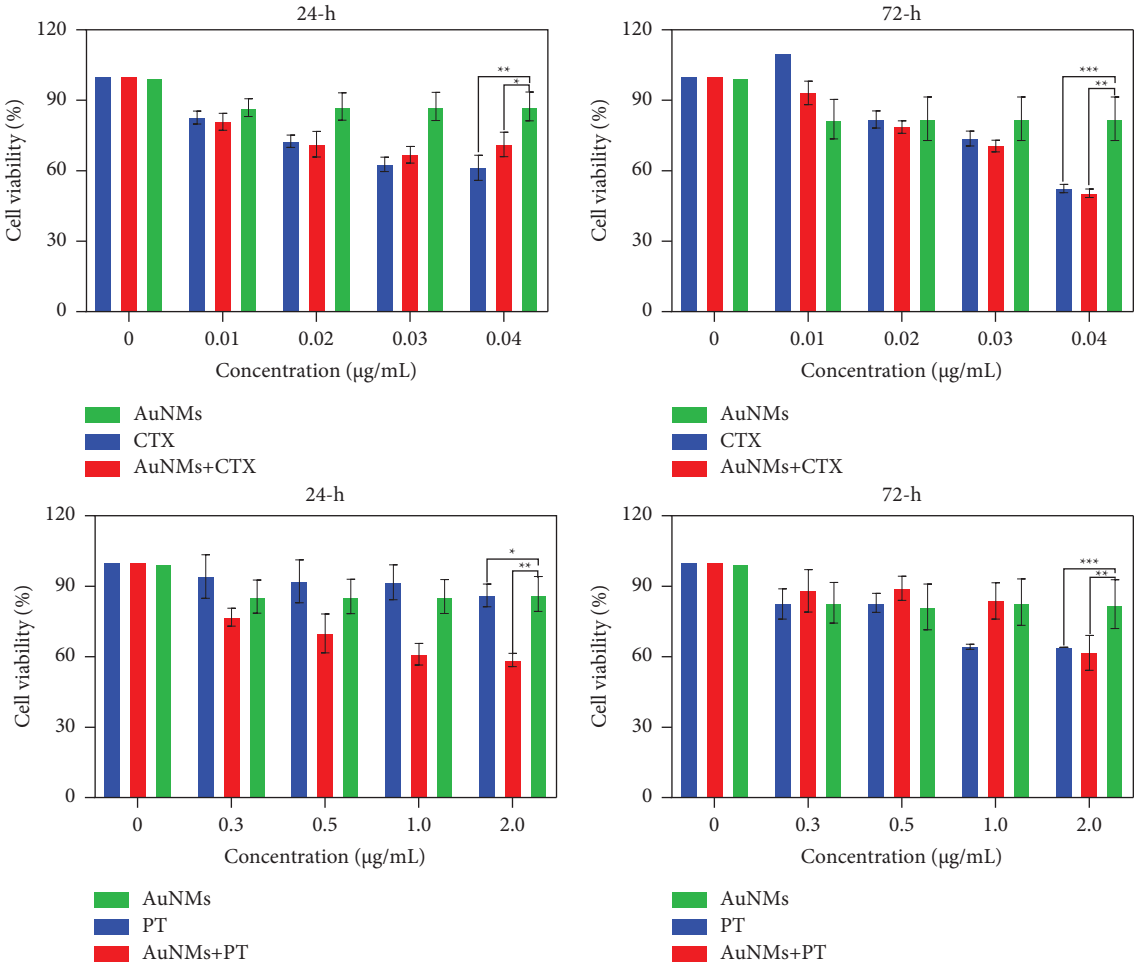

Figure 3: In vitro cytotoxicity of the AuNMs, free CTX, free PT, AuNMs@CTX, and AuNMs@PT was investigated by the MTT assay using U87 glioma cancer cells for 24 and 72 h. Data were expressed as means ± SEM ($n = 3$). ($^{*}P < 0.05$, $^{**}P < 0.01$, $^{***}P < 0.001$).

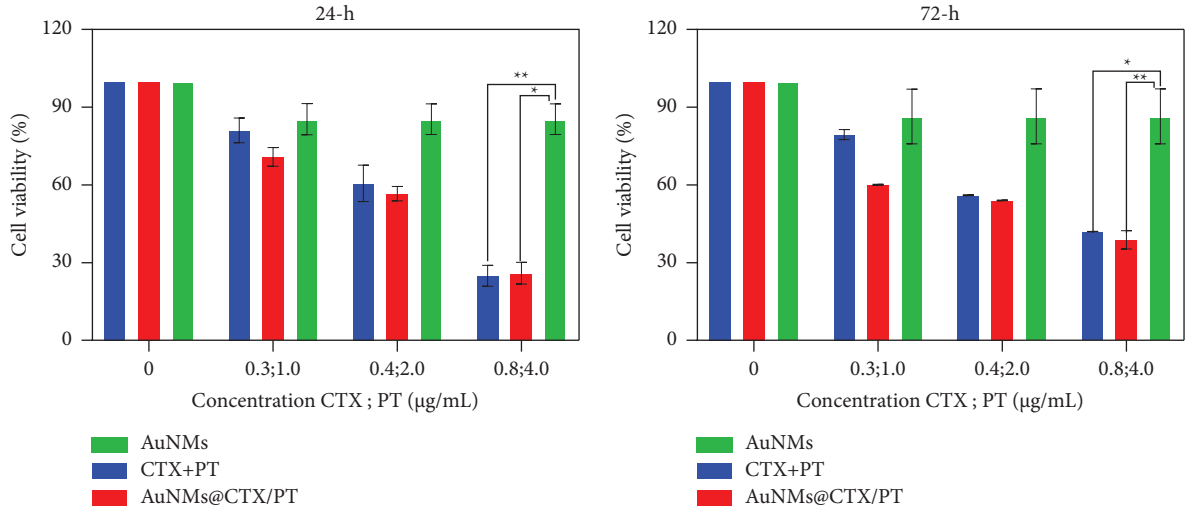

Figure 4: In vitro cytotoxicity of the AuNMs, CTX + PT, and AuNMs@CTX/PT was investigated by the MTT assay using U87 glioma cancer cells for 24 and 72 h. Data were expressed as means ± SEM ($n = 3$). ($^{*}P < 0.05$, $^{**}P < 0.01$).

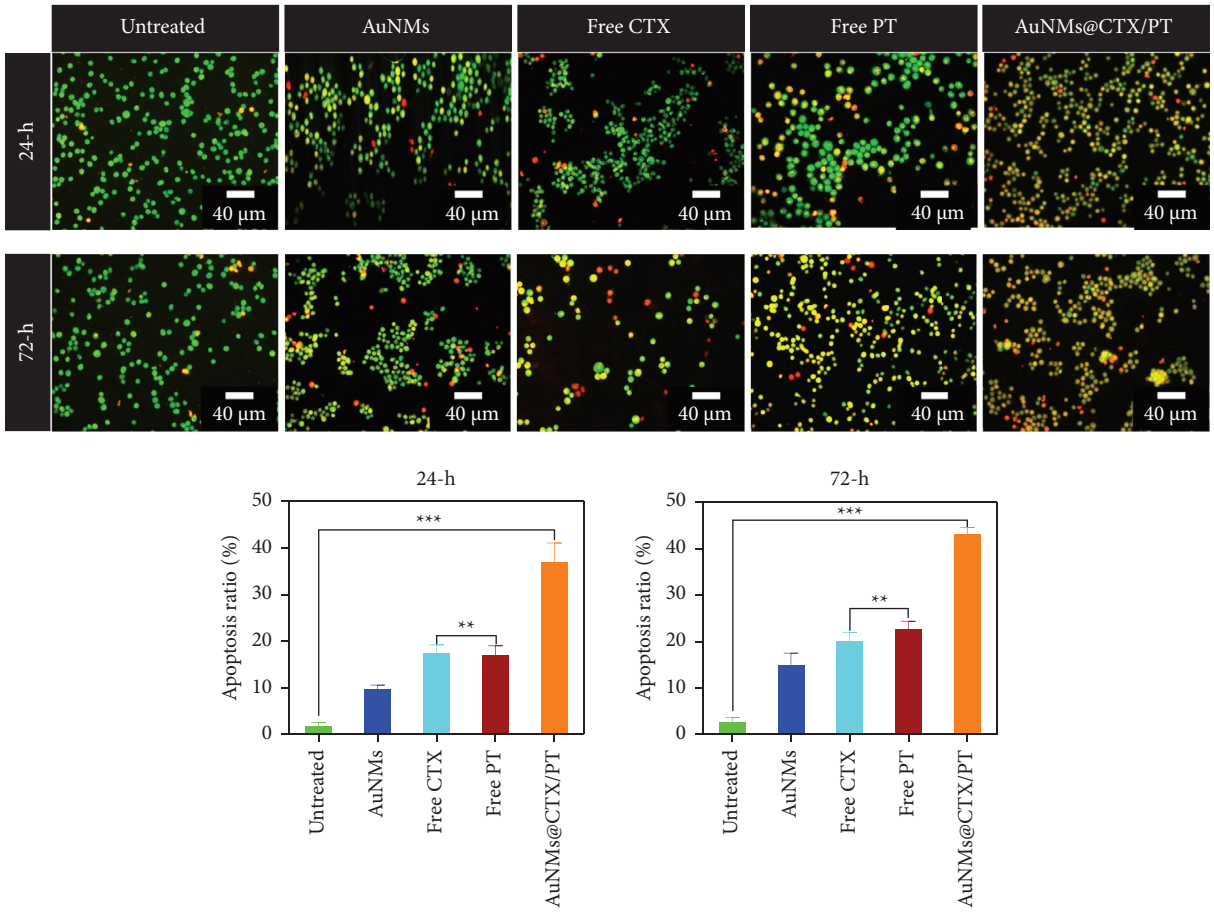

Figure 5: The morphological changes of the AuNMs, free CTX, free PT, and AuNMs@CTX/PT. AO-EB staining of AuNMs, free CTX, free PT, and AuNMs@CTX/PT treated with U87 glioma cancer cells for 24 and 72 h. Scale bar 40 μm. Data were expressed as means ± SEM ($n = 3$). ($^{**}P < 0.01$, $^{***}P < 0.001$).

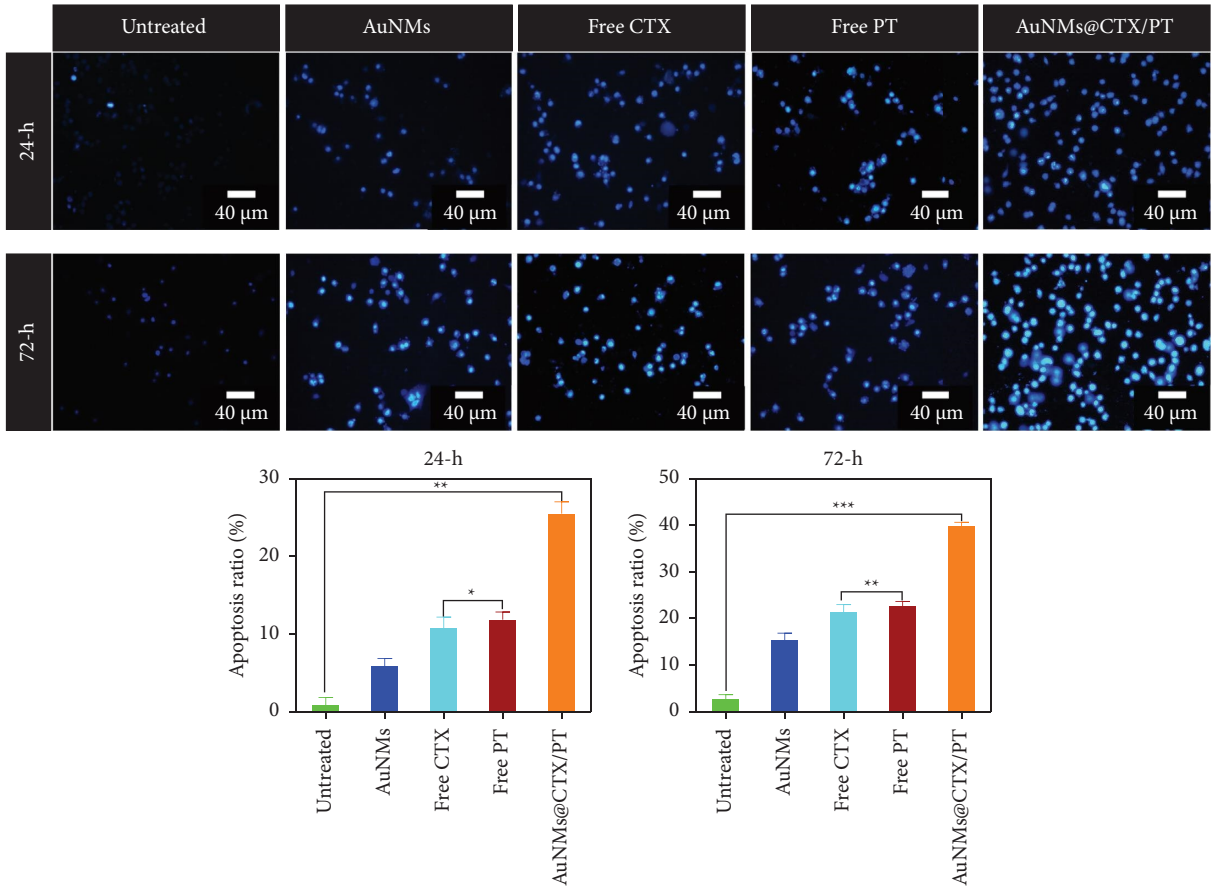

Figure 6: The nuclear morphology changes of the AuNMs, free CTX, free PT, and AuNMs@CTX/PT. DAPI staining of AuNMs, free CTX, free PT, and AuNMs@CTX/PT treated with U87 glioma cancer cells for 24 and 72 h. Scale bar 40 μm. Data were expressed as means ± SEM ($n = 3$). ($^{*}P < 0.05$, $^{**}P < 0.01$, $^{***}P < 0.001$).

3.3. Apoptosis Investigation. The physical feature of chromatin condensation in the stained nucleus and the differential uptake of fluorescent DNA binding dyes acridine orange and ethidium bromide are utilized in the acridine orange (AO)/ethidium bromide (EB) double staining approach [58–62]. AuNMs, free CTX, free PT, and AuNMs@CTX/PT toxicity led to a decrease in viable cells (VN) and an increase in early apoptotic (VA), late apoptotic (NVA), and necrotic cells (NVN). AO/EB labelling tracked the apoptosis rate in U87 glioma cancer cells after they were treated with AuNMs, free CTX, free PT, and AuNMs@CTX/PT (Figure 5). The data show that both early and late apoptotic cells are present in IC_{50}-treated cells with 24 and 72 h (Figure 5). Green with numerous orange spots indicated chromatin condensation and nuclear disintegration in early apoptotic cells. Orange staining of late apoptotic cells was indicative of condensed and shattered nuclei. The untreated (control) cells kept their green colour and regular shape. Nuclear staining with DAPI was conducted to provide context for the findings (Figure 6). Figure 6 demonstrates that after staining with DAPI, cells treated with 24 and 72 h to the IC_{50} concentrations of AuNMs, free CTX, free PT, and AuNMs@CTX/PT had a higher number of nuclear fragmentations than the control group. The findings corroborated those from the dual staining method.

The three main types of cell death are apoptosis, autophagy, and necrosis. An apoptosis kit including PI and FITC-labeled annexin-V dye was used to examine the cancer cells' apoptosis [14]. During the apoptosis stage, phosphatidylserine (PS) exposed outside the cell can be highly explicitly bound by the annexin V dye. According to the findings, the U87 cells' apoptosis rate increased following stimulation with AuNMs, free CTX, free PT, AuNMs@CTX/PT, and AuNMs@CTX/PT. Apoptosis also increased with the concentration of the AuNMs@CTX/PT (Figure 7). The cells were exposed for 24 and 72 h to the IC_{50} concentrations of AuNMs, free CTX, free PT, and AuNMs@CTX/PT to calculate the percentage of apoptotic and necrotic cells. In this case, we discovered that AuNMs@CTX/PT could cause apoptosis in U87 cells. The findings of the flow cytometry analysis demonstrated that the IC_{50} concentration of AuNMs@CTX/PT increased the apoptosis rate in the treated cells (Figure 7).

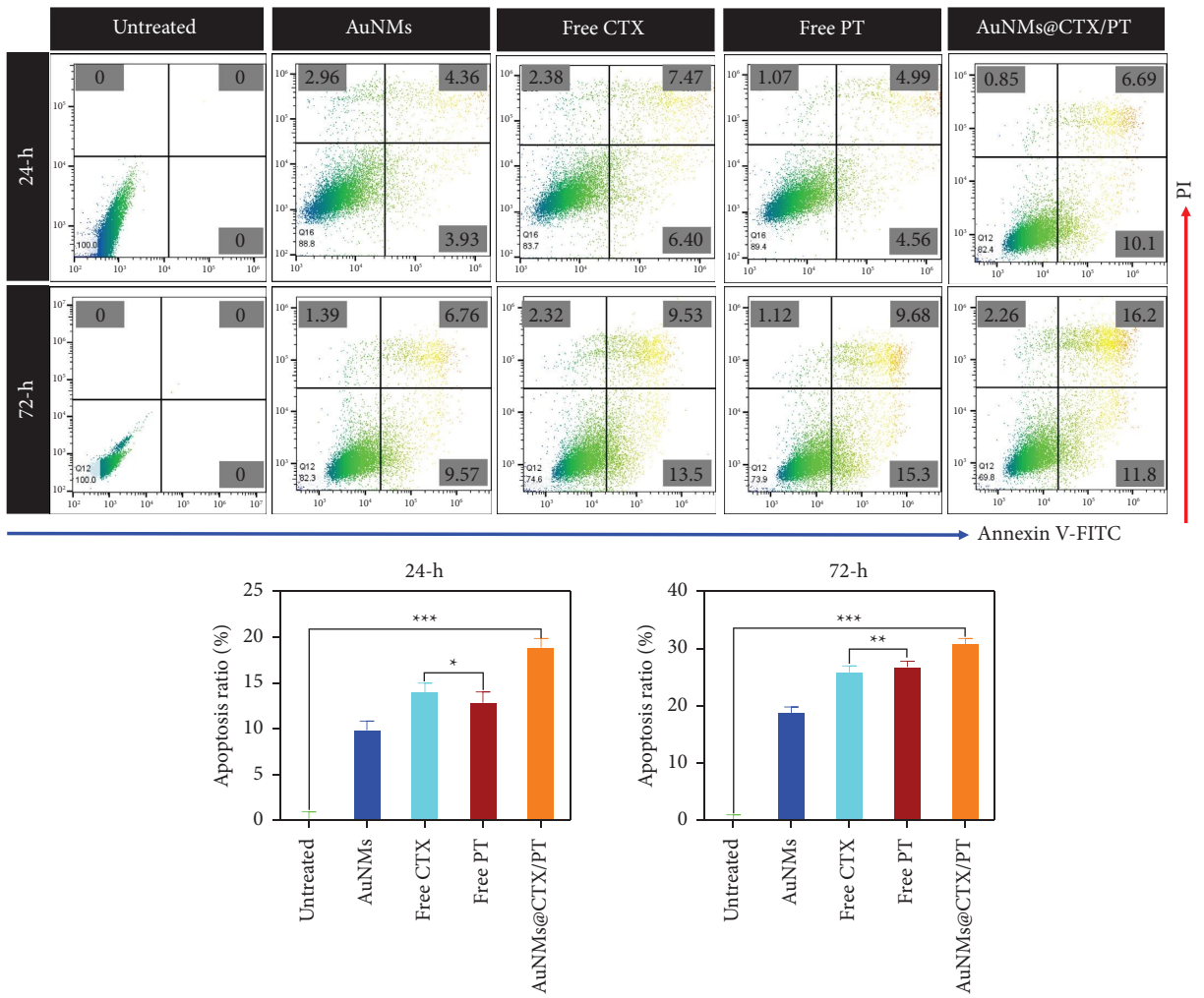

Figure 7: The apoptosis of the AuNMs, free CTX, free PT, and AuNMs@CTX/PT were confirmed by flow cytometry analysis. The U87 glioma cancer cells were stained with Annexin V-FITC and PI for 24 and 72 h. Data were expressed as means ± SEM ($n = 3$). ($^{*}P < 0.05$, $^{**}P < 0.01$, $^{***}P < 0.001$).

4. Conclusion

These studies show that CTX and PT, in conjunction with AuNMs, can be an effective therapeutic strategy. Nanomaterials' size on the nanometer scale, high colloidal stability, and negative zeta potential were all characteristics. The particle size of gold nanomaterials was about ~20 nm. Our data demonstrated that the cytotoxic effect of the drugs in combination with AuNMs on U87 cells was greater than that of the CTX and PT drugs. AuNMs@CTX/PT results of cytotoxicity tests in vitro had good biocompatibility. The biochemical apoptosis staining techniques investigated the cells' morphological changes of the cells (AO-EB and nuclear (DAPI) staining techniques). Furthermore, the flow cytometry analysis examined the mode of cell death. Thus, this exploration indicates that the fabricated AuNMs@CTX/PT may deliver an excellent idea for fabrication and improve biocompatible and safe nanomaterials that can carry a wide range of therapeutic agents to treat glioma cancer.

Data Availability

All data generated or analyzed during this study are included within the article. The raw data shall be made available upon request from the corresponding author.

Conflicts of Interest

The authors declare that they have no conflicts of interest.

Authors' Contributions

The manuscript was written through the contributions of all authors. All authors have approved the final version of the manuscript.

Acknowledgments

The authors extend their appreciation to the researchers supporting project number (RSPD2023R677) King Saud University, Riyadh, Saudi Arabia, for financial support.

References

[1] Y. Tülüce, P. T. A. Lak, İ. Koyuncu, A. Kılıç, M. Durgun, and H. Özkol, "The apoptotic, cytotoxic and genotoxic effect of novel binuclear boron-fluoride complex on endometrial cancer," *Biometals*, vol. 30, no. 6, pp. 933–944, 2017.

[2] Y. Tuluce, H. N. Mohammed, İ. Koyuncu, A. Kiliç, and M. Durgun, "ROS-Mediated genotoxicity and apoptosis induced by a novel salicylaldimine derivatives in human cervical cancer cells," *Current Medicinal Chemistry*, vol. 30, no. 33, pp. 3815–3829, 2023.

[3] Y. Tülüce, A. I. Hussein, İ. Koyuncu, A. Kilic, and M. Durgun, "The effect of a bis-structured Schiff base on apoptosis, cytotoxicity, and DNA damage of breast cancer cells," *Journal of Biochemical and Molecular Toxicology*, vol. 36, no. 10, Article ID e23148, 2022.

[4] Y. Tülüce, H. D. I. Masseh, İ. Koyuncu, A. Kiliç, M. Durgun, and H. Özkol, "Novel fluorine boron hybrid complex as potential antiproliferative drugs on colorectal cancer cell line," *Anti-Cancer Agents in Medicinal Chemistry*, vol. 19, no. 5, pp. 627–637, 2019.

[5] A. Kilic, I. Koyuncu, M. Durgun, I. Ozaslan, İ. H. Kaya, and A. Gönel, "Synthesis and characterization of the hemi-salen ligands and their triboron complexes: spectroscopy and examination of anticancer properties," *Chemistry and Biodiversity*, vol. 15, no. 1, Article ID e1700428, 2018.

[6] G. Lombardi, V. Barresi, A. Castellano et al., "Clinical management of diffuse low-grade gliomas," *Cancers*, vol. 12, no. 10, p. 3008, 2020.

[7] J. Li, T. Tan, L. Zhao et al., "Recent advancements in liposome-targeting strategies for the treatment of gliomas: a systematic review," *ACS Applied Bio Materials*, vol. 3, no. 9, pp. 5500–5528, 2020.

[8] B. S. Mahmoud, A. H. AlAmri, and C. McConville, "Polymeric nanoparticles for the treatment of malignant gliomas," *Cancers*, vol. 12, no. 1, p. 175, 2020.

[9] K. Masliantsev, L. Karayan-Tapon, and P.-O. Guichet, "Hippo signaling pathway in gliomas," *Cells*, vol. 10, no. 1, p. 184, 2021.

[10] G. Youssef and J. J. Miller, "Lower grade gliomas," *Current Neurology and Neuroscience Reports*, vol. 20, no. 7, pp. 21–29, 2020.

[11] J. P. Fisher and D. C. Adamson, "Current FDA-approved therapies for high-grade malignant gliomas," *Biomedicines*, vol. 9, no. 3, p. 324, 2021.

[12] G. Singh, S. Manjila, N. Sakla et al., "Radiomics and radiogenomics in gliomas: a contemporary update," *British Journal of Cancer*, vol. 125, no. 5, pp. 641–657, 2021.

[13] M. J. Mair, M. Geurts, M. J. van den Bent, and A. S. Berghoff, "A basic review on systemic treatment options in WHO grade II-III gliomas," *Cancer Treatment Reviews*, vol. 92, Article ID 102124, 2021.

[14] Y. Zeng, H. Chen, F. Yang, H. Li, and P. Yang, "A feasible strategy of fabricating camptothecin (SN38)-loaded holmium ferrite nanocarrier delivery for glioma treatment," *Materials Research Express*, vol. 9, no. 11, Article ID 115011, 2022.

[15] A. C. Freeman, S. R. Platt, S. Holmes et al., "Convection-enhanced delivery of cetuximab conjugated iron-oxide nanoparticles for treatment of spontaneous canine intracranial gliomas," *Journal of Neuro-Oncology*, vol. 137, no. 3, pp. 653–663, 2018.

[16] H. Hua, X. Zhang, H. Mu et al., "RVG29-modified docetaxel-loaded nanoparticles for brain-targeted glioma therapy," *International Journal of Pharmaceutics*, vol. 543, no. 1-2, pp. 179–189, 2018.

[17] R. Afzalipour, S. Khoei, S. Khoee et al., "Thermosensitive magnetic nanoparticles exposed to alternating magnetic field and heat-mediated chemotherapy for an effective dual therapy in rat glioma model," *Nanomedicine: Nanotechnology, Biology and Medicine*, vol. 31, Article ID 102319, 2021.

[18] H. Shi, S. Sun, H. Xu et al., "<p>Combined delivery of temozolomide and siPLK1 using targeted nanoparticles to enhance temozolomide sensitivity in glioma</p&gt," *International Journal of Nanomedicine*, vol. 15, pp. 3347–3362, 2020.

[19] R. Afzalipour, S. Khoei, S. Khoee et al., "Dual-targeting temozolomide loaded in folate-conjugated magnetic triblock copolymer nanoparticles to improve the therapeutic efficiency of rat brain gliomas," *ACS Biomaterials Science & Engineering*, vol. 5, no. 11, pp. 6000–6011, 2019.

[20] J. Zhao, P. Liu, J. Ma et al., "<p>Enhancement of radiosensitization by silver nanoparticles functionalized with polyethylene glycol and aptamer As1411 for glioma irradiation therapy</p&gt," *International Journal of Nanomedicine*, vol. 14, pp. 9483–9496, 2019.

[21] Y. Cui, J. Sun, W. Hao et al., "Dual-target peptide-modified erythrocyte membrane-enveloped PLGA nanoparticles for the treatment of glioma," *Frontiers in Oncology*, vol. 10, Article ID 563938, 2020.

[22] X. Wang, J. Gao, X. Ouyang, J. Wang, X. Sun, and Y. Lv, "Mesenchymal stem cells loaded with paclitaxel– poly(lactic-co-glycolic acid) nanoparticles for glioma-targeting therapy," *International Journal of Nanomedicine*, vol. 13, pp. 5231–5248, 2018.

[23] J. Zhang, Z. Zhang, M. Jiang et al., "Developing a novel gold (III) agent to treat glioma based on the unique properties of apoferritin nanoparticles: inducing lethal autophagy and apoptosis," *Journal of Medicinal Chemistry*, vol. 63, no. 22, pp. 13695–13708, 2020.

[24] L. Hua, Z. Wang, L. Zhao et al., "Hypoxia-responsive lipid-poly-(hypoxic radiosensitized polyprodrug) nanoparticles for glioma chemo-and radiotherapy," *Theranostics*, vol. 8, no. 18, pp. 5088–5105, 2018.

[25] M. Norouzi, "Gold nanoparticles in glioma theranostics," *Pharmacological Research*, vol. 156, Article ID 104753, 2020.

[26] M. T. Luiz, L. B. Tofani, V. H. S. Araújo et al., "Gene therapy based on lipid nanoparticles as non-viral vectors for Glioma treatment," *Current Gene Therapy*, vol. 21, no. 5, pp. 452–463, 2021.

[27] J. Li, J. Zhao, T. Tan et al., "<p>Nanoparticle drug delivery system for glioma and its efficacy improvement strategies: a comprehensive review</p&gt," *International Journal of Nanomedicine*, vol. 15, pp. 2563–2582, 2020.

[28] Y.-B. Pan, S. Wang, X. He et al., "A combination of glioma in vivo imaging and in vivo drug delivery by metal–organic framework based composite nanoparticles," *Journal of Materials Chemistry B*, vol. 7, no. 48, pp. 7683–7689, 2019.

[29] Q. Lu, X. Dai, P. Zhang et al., "Fe<sub&gtx;3</sub>-O₄@Au composite magnetic nanoparticles modified with cetuximab for targeted magneto-photothermal therapy of glioma cells," *International Journal of Nanomedicine*, vol. 13, pp. 2491–2505, 2018.

[30] J. Wan, X. Ma, D. Xu, B. Yang, S. Yang, and S. Han, "Docetaxel-decorated anticancer drug and gold nanoparticles encapsulated apatite carrier for the treatment of liver cancer," *Journal of Photochemistry and Photobiology B: Biology*, vol. 185, pp. 73–79, 2018.

[31] K. Doello, C. Mesas, G. Perazzoli et al., "The expression of MMR, CD133 and the presence of p53 wt predict the response to cabazitaxel in malignant neural tumours cell lines," *Annals of Oncology*, vol. 30, p. 16, 2019.

[32] P. E. Manley, T. Trippett, A. A. Smith et al., "A phase 1/2 dose-finding, safety, and activity study of cabazitaxel in pediatric patients with refractory solid tumors including tumors of the central nervous system," *Pediatric Blood and Cancer*, vol. 65, no. 9, Article ID e27217, 2018.

[33] E. Sulheim, Y. Mørch, S. Snipstad et al., "Therapeutic effect of cabazitaxel and blood-brain barrier opening in a patient-derived glioblastoma model," *Nanotheranostics*, vol. 3, no. 1, pp. 103–112, 2019.

[34] S. Wu, L. Lu, J. Zhou et al., "All-stage targeted therapy for glioblastoma based on lipid membrane coated cabazitaxel nanocrystals," *Journal of Controlled Release*, vol. 345, pp. 685–695, 2022.

[35] C. Chen, R. Fan, Y. Wang et al., "Hyaluronic acid-conjugated nanoparticles for the targeted delivery of cabazitaxel to CD44-overexpressing glioblastoma cells," *Journal of Biomedical Nanotechnology*, vol. 17, no. 4, pp. 595–605, 2021.

[36] J. Li, H. Zeng, Y. You et al., "Active targeting of orthotopic glioma using biomimetic liposomes co-loaded elemene and cabazitaxel modified by transferritin," *Journal of Nanobiotechnology*, vol. 19, pp. 289–319, 2021.

[37] S. Sharabi, D. Guez, D. Daniels et al., "The application of point source electroporation and chemotherapy for the treatment of glioma: a randomized controlled rat study," *Scientific Reports*, vol. 10, pp. 2178–2212, 2020.

[38] S. Tang, Y. Gao, and W. Hu, "Scutellarin inhibits the metastasis and cisplatin resistance in glioma cells," *OncoTargets and Therapy*, vol. 12, pp. 587–598, 2019.

[39] J. Jeon, S. Lee, H. Kim et al., "Revisiting platinum-based anticancer drugs to overcome gliomas," *International Journal of Molecular Sciences*, vol. 22, no. 10, p. 5111, 2021.

[40] Y. Ma, G. Zhou, M. Li et al., "Long noncoding RNA DANCR mediates cisplatin resistance in glioma cells via activating AXL/PI3K/Akt/NF-κB signaling pathway," *Neurochemistry International*, vol. 118, pp. 233–241, 2018.

[41] B. Björkblom, P. Jonsson, P. Tabatabaei et al., "Metabolic response patterns in brain microdialysis fluids and serum during interstitial cisplatin treatment of high-grade glioma," *British Journal of Cancer*, vol. 122, no. 2, pp. 221–232, 2020.

[42] W.-Q. Cao, X.-Q. Zhai, J.-W. Ma et al., "Natural borneol sensitizes human glioma cells to cisplatin-induced apoptosis by triggering ROS-mediated oxidative damage and regulation of MAPKs and PI3K/AKT pathway," *Pharmaceutical Biology*, vol. 58, no. 1, pp. 72–79, 2020.

[43] J. Enríquez Pérez, S. Fritzell, J. Kopecky, E. Visse, A. Darabi, and P. Siesjö, "The effect of locally delivered cisplatin is dependent on an intact immune function in an experimental glioma model," *Scientific Reports*, vol. 9, pp. 5632–5710, 2019.

[44] Z. Jing, M. Li, H. Wang et al., "Gallic acid-gold nanoparticles enhance radiation-induced cell death of human glioma U251 cells," *IUBMB Life*, vol. 73, no. 2, pp. 398–407, 2021.

[45] L. Zhao, Y. Li, J. Zhu et al., "Chlorotoxin peptide-functionalized polyethylenimine-entrapped gold nanoparticles for glioma SPECT/CT imaging and radionuclide therapy," *Journal of Nanobiotechnology*, vol. 17, no. 1, p. 30, 2019.

[46] A. Neshastehriz, Z. Khosravi, H. Ghaznavi, and A. Shakeri-Zadeh, "Gold-coated iron oxide nanoparticles trigger apoptosis in the process of thermo-radiotherapy of U87-MG human glioma cells," *Radiation and Environmental Biophysics*, vol. 57, no. 4, pp. 405–418, 2018.

[47] S. Ruan, R. Xie, L. Qin et al., "Aggregable nanoparticles-enabled chemotherapy and autophagy inhibition combined with anti-PD-L1 antibody for improved glioma treatment," *Nano Letters*, vol. 19, no. 11, pp. 8318–8332, 2019.

[48] D. F. Báez, E. Gallardo-Toledo, M. P. Oyarzún, E. Araya, and M. J. Kogan, "The influence of size and chemical composition of silver and gold nanoparticles on in vivo toxicity with potential applications to central nervous system diseases," *International Journal of Nanomedicine*, vol. 16, pp. 2187–2201, 2021.

[49] V. Delplace, P. Couvreur, and J. Nicolas, "Recent trends in the design of anticancer polymer prodrug nanocarriers," *Polymer Chemistry*, vol. 5, pp. 1529–1544, 2014.

[50] M. J. Bruining, H. Gt Blaauwgeers, R. Kuijer, E. Pels, R. M. M. A. Nuijts, and L. H. Koole, "Biodegradable three-dimensional networks of poly(dimethylamino ethyl methacrylate). Synthesis, characterization and in vitro studies of structural degradation and cytotoxicity," *Biomaterials*, vol. 21, no. 6, pp. 595–604, 2000.

[51] E. Waleka, M. Mackiewicz, J. Romanski, A. Dybko, Z. Stojek, and M. Karbarz, "Degradable nanohydrogel with high doxorubicin loadings exhibiting controlled drug release and decreased toxicity against healthy cells," *International Journal of Pharmaceutics*, vol. 579, Article ID 119188, 2020.

[52] A. Golchin, S. Hosseinzadeh, M. Staji, M. Soleimani, A. Ardeshirylajimi, and A. Khojasteh, "Biological behavior of the curcumin incorporated chitosan/poly(vinyl alcohol) nanofibers for biomedical applications," *Journal of Cellular Biochemistry*, vol. 120, no. 9, pp. 15410–15421, 2019.

[53] Y. Hu, D. Yu, and X. Zhang, "9-amino acid cyclic peptide-decorated sorafenib polymeric nanoparticles for the efficient in vitro nursing care analysis of hepatocellular carcinoma," *Process Biochemistry*, vol. 100, pp. 140–148, 2021.

[54] T. Sathiya Kamatchi, M. K. Mohamed Subarkhan, R. Ramesh, H. Wang, and J. G. Małecki, "Investigation into anti-proliferative activity and apoptosis mechanism of new arene Ru(ii) carbazole-based hydrazone complexes," *Dalton Transactions*, vol. 49, no. 32, pp. 11385–11395, 2020.

[55] K. Giriraj, M. S. Mohamed Kasim, K. Balasubramaniam et al., "Various coordination modes of new coumarin Schiff bases toward Cobalt (III) ion: synthesis, spectral characterization, in vitro cytotoxic activity, and investigation of apoptosis," *Applied Organometallic Chemistry*, vol. 36, no. 3, Article ID e6536, 2022.

[56] S. Kasibhatla, G. P. Amarante-Mendes, D. Finucane, T. Brunner, E. Bossy-Wetzel, and D. R. Green, "Acridine orange/ethidium bromide (AO/EB) staining to detect apoptosis," *Cold Spring Harbour Protocols*, vol. 2006, no. 3, pp. 493–803, 2006.

[57] M. F. Sanad, E. S. Abu Serea, S. M. Bazid, S. Nabih, M. A. Ahsan, and A. E. Shalan, "High cytotoxic activity of ZnO@leucovorin nanocomposite based materials against an MCF-7 cell model," *Analytical Methods*, vol. 12, no. 16, pp. 2176–2184, 2020.

[58] D. P. Dorairaj, J. Haribabu, M. Dharmasivam et al., "Ru(II)-p-Cymene complexes of furoylthiourea ligands for anticancer applications against breast cancer cells," *Inorganic Chemistry*, vol. 62, no. 30, pp. 11761–11774, 2023.

[59] M. K. M. Subarkhan and R. Ramesh, "Ruthenium(II) arene complexes containing benzhydrazone ligands: synthesis, structure and antiproliferative activity," *Inorganic Chemistry Frontiers*, vol. 3, no. 10, pp. 1245–1255, 2016.

[60] M. S. Mohamed Kasim, S. Sundar, and R. Rengan, "Synthesis and structure of new binuclear ruthenium(ii) arene benzil bis(benzoylhydrazone) complexes: investigation on antiproliferative activity and apoptosis induction," *Inorganic Chemistry Frontiers*, vol. 5, no. 3, pp. 585–596, 2018.

[61] S. Swaminathan, J. Haribabu, M. K. Mohamed Subarkhan et al., "Coordination behavior of acylthiourea ligands in their Ru(II)–Benzene Complexes─Structures and anticancer activity," *Organometallics*, vol. 41, no. 13, pp. 1621–1630, 2022.

[62] S. Swaminathan, J. Haribabu, M. K. Mohamed Subarkhan et al., "Impact of aliphatic acyl and aromatic thioamide substituents on the anticancer activity of Ru(ii)-p-cymene complexes with acylthiourea ligands—in vitro and in vivo studies," *Dalton Transactions*, vol. 50, no. 44, pp. 16311–16325, 2021.